Article

Critical Role of Layer Thickness in Frontal Polymerization

Reda Tiani,* John A. Pojman, and Laurence Rongy*

Cite This: *J. Phys. Chem. B* 2022, 126, 3607−3618

Read Online

ACCESS |

Metrics & More

Article Recommendations

ABSTRACT: Thermal frontal polymerization (FP) is a chemical process during which a cold monomer−initiator mixture is converted into a hot polymer as a polymerization front propagates in the system due to the interplay between heat diffusion and the exothermicity of the reaction. The theoretical description of FP generally focuses on one-dimensional (1D) reaction−diffusion (RD) models where the effect of heat losses is encoded into an effective parameter in the heat equation. We show here the limits of such 1D models to describe FP under nonadiabatic conditions. To do so, the propagation of a polymerization front is analyzed both analytically and numerically in a rectangular two-dimensional (2D) layer. The layer thickness is shown to control the dynamics of the front and to determine its very existence. We find that for given heat losses, a minimum thickness is required for front propagation as recently observed in FP experiments of 2D thin films on wood. Moreover, when the thickness exceeds a critical value, the front is observed to survive independently of the rate of heat losses. This result cannot be predicted with 1D models where front extinction is always possible. A scaling analysis is proposed to highlight the physical interpretation of such a front survival. The influence of dimensionality on thermal instabilities is also analyzed, with a focus on the differences with the 1D predictions.
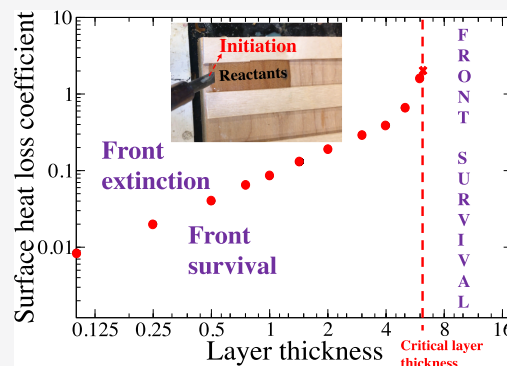
INTRODUCTION

In the last few years, great interest has been devoted to the study of thermal frontal polymerization (FP), defined as a self-sustained chemical process in which a cold monomer−initiator mixture (around 300 K) is converted into a hot polymer (around 500 K) via a localized reaction zone that propagates due to the interplay between heat diffusion and exothermic polymerization.[1,2] FP is initiated by the local application of a heat source and can be achieved when the polymerization reaction has a negligible rate at ambient temperature but a high rate of conversion at the front temperature. Additionally, the reaction has to release heat faster than it is lost to the environment.[2,3] FP has been successfully applied to the synthesis of materials, including nanocomposites,[4,5] hydrogels,[6−8] sensory materials,[9,10] and fiber-reinforced polymer composites (FRPCs).[11−13] In particular, Robertson et al.[11] showed that FP allows a fast, energy-efficient, and greener synthesis of high-performance thermosets and FRPCs, such as the ones used in chemical, aerospace, and wind turbines industries, compared to traditional autoclave- or oven-based manufacturing techniques.

Most of the theoretical works on FP are based on one-dimensional (1D) reaction−diffusion (RD) models, both under adiabatic[3,14−18] and nonadiabatic conditions,[19−24] to describe the front dynamics with a large focus on thermal instabilities arising from the loss of stability of a steady state. However, 1D models cannot fully explain recent experimental results. In particular, Bansal et al.[25] explored the possibility to use FP as a

technique to form two-dimensional (2D) thin films (<0.5 mm) on wood for promising applications in thin films or coatings. The authors noted that the front propagates above a minimal value of the layer thickness and of the viscosity of the monomer−initiator mixture. Goli et al.[26] experimentally and numerically investigated the role of a conductive fiber (stainless steel or copper) embedded inside a cylindrical microchannel on FP. Similarly to the study of Bansal et al.,[25] the authors also found experimentally that a critical value of the microchannel radius was needed for FP to occur. They related that to the presence of heat losses to the medium (a polydimethylsiloxane matrix) surrounding the microchannel. Using a glass test tube, Frulloni et al.[27] performed an experiment on FP of an epoxy system and built a 2D RD model to supplement their experiment. The values of the model parameters were obtained by fitting the experiments. Only recently, a more detailed parametric study of the impact of heat losses on a polymerization front in a rectangular channel with a dicyclopentadiene (DCPD) monomer was conducted by Goli et al.[28] In particular, when heat losses occur along the contact interface between the channel and a conductive tool plate, the

authors mentioned that in the limit of a very large plate of infinite thermal diffusivity, the front propagates above a critical value of the height of the channel despite large heat losses.

In the above literature, we note that the analysis of the role of dimensionality on FP was preliminary while the authors focused more on the role of heat losses on FP. Also, the models were generally tailored to fit an experiment and the values of the parameters were typically restricted in the range of the corresponding experiment. As far as we know, the importance of dimensionality in FP and the fundamental connections and differences with the predictions of 1D RD models[19−21] have not been highlighted yet in the literature.

In this context, we seek a generic RD model to study the effect of heat losses on FP in two dimensions. To do so, we assume a rectangular layer in which a monomer−initiator mixture is converted into a polymer via FP and where heat losses to the environment can occur through one of the system boundaries (either the surface or the system bottom). This model can be viewed as a prototype model for the experiments of Bansal et al.,[25] but is not restricted to it, in the limit of infinitely large viscosity of the monomer−initiator mixture so that the possible role of natural convection can be neglected. In the absence of heat losses, the temperature and the chemical concentrations are independent of the layer thickness due to translational symmetry and are thus exact solutions of a 1D RD model. When heat losses occur, such a translational symmetry is broken and we show that the layer thickness critically affects the front dynamics. The connection with the predictions of 1D RD models and the departure from the latter are presented, with a particular focus on the physical interpretation of the role of the layer thickness on the system dynamics. Our results corroborate qualitatively the ones of Goli et al.[28] about the influence of heat losses and of the channel width on the maximum temperature and front speed. In particular, we provide more detailed insights into the possibility of front survival independently of heat losses based on a scaling analysis.

The article is organized as follows. We first present the model system and the corresponding 2D governing equations. To compare with the predictions based on 1D RD models, we next analyze the 2D equations in the 1D limit, i.e., for an infinitely small layer thickness. The numerical solutions of the 2D nonadiabatic models for arbitrary values of the layer thickness are then analyzed. The dependence of the nonadiabatic front dynamics on the heating time is discussed next. The influence of dimensionality is also investigated on thermal instabilities. Eventually, conclusions and prospects are drawn and extensions to the case of two horizontal conductive boundaries are presented.

■ THEORY

We consider a 2D system of length L_x and thickness L_z that contains initially a monomer−initiator mixture. Due to the application of a heat source at the left system boundary, for instance, with a thermoelectric heater or with a heat gun,[2,25] the cold monomer−initiator mixture is converted into a hot polymer by free-radical polymerization as a spatially localized reaction zone (called a polymerization front) propagates in the system (see Figure 1). The governing equations are the kinetic equations for the monomer $M(x, z, t)$ and the initiator $I(x, z, t)$ concentrations, coupled to the heat RD equation. This so-called three-step FP kinetic model has been used extensively in the literature for the study of free-radical polymerizations with a
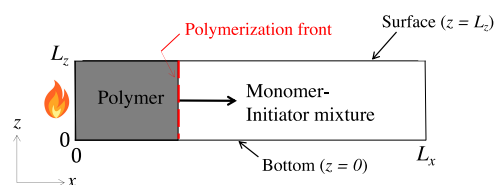

Figure 1. Sketch of the system. The polymerization front is the reactive interface in which a cold monomer−initiator mixture is converted into a hot polymer as the front propagates in the system that consists of two horizontal boundaries, the surface ($z = L_z$) and the bottom ($z = 0$), and two lateral boundaries, the left ($x = 0$) and right ($x = L_x$) boundaries. The front is initiated with a heat source illustrated as a burning flame at the left system boundary.

thermal initiator, especially in 1D systems.[18−21] The equations write

$$\frac{\partial I}{\partial t} = -k_d(T)I \tag{1}$$

$$\frac{\partial M}{\partial t} = -k_{eff}(T)M\sqrt{I} \tag{2}$$

$$\rho_0 c_p \frac{\partial T}{\partial t} = \lambda \nabla^2 T - \Delta H \, k_{eff}(T)M\sqrt{I} \tag{3}$$

where $T(x, z, t)$ is the temperature and the Laplacian operator is defined by $\nabla^2 = \partial^2/\partial x^2 + \partial^2/\partial z^2$. The solution density ρ_0, the specific heat capacity c_p, the thermal conductivity λ, and the reaction enthalpy per mole of monomer ΔH (here negative since the polymerization reaction is exothermic) are all assumed constant. The rate constant $k_d(T)$ and the effective one, $k_{eff}(T)$, associated with the initiator decomposition and the monomer consumption, respectively, follow the Arrhenius equation, that is, $k_j(T) = k_j^0 \exp(-E_j/RT)$, where k_j^0 is the preexponential factor and $j = d$ or eff. We note that eqs 1 and 2 do not include diffusion terms since mass diffusion can be neglected with respect to heat diffusion.[18] We have also assumed here that the viscosity of the monomer−initiator mixture, which can easily be controlled in experiments,[25] is infinitely large so as to prevent any convective motion.

Our rectangular system consists of two lateral boundaries, the left ($x = 0$) and right ($x = L_x$) boundaries, and two horizontal boundaries, the upper ($z = L_z$) and lower ($z = 0$) boundaries (see Figure 1). To initiate the polymerization front, we impose a constant temperature T_s at $x = 0$. At $z = L_z$, we assume heat losses to occur to the surrounding. This is equivalent to assuming heat losses from the bottom of the system rather than from the surface, due to symmetry. At $z = 0$ and $x = L_x$, the boundaries are taken thermally insulated. We note that the boundary conditions (BC) at the right system boundary ($x = L_x$) do not influence the system dynamics on the times considered because L_x is taken sufficiently large. For the chemical concentrations, we require zero-flux boundary conditions at each boundary. The boundary conditions (BCs) therefore read, for all times,

$$\frac{\partial M}{\partial x} = 0 = \frac{\partial I}{\partial x}, \ T = T_s \text{ at } x = 0 \tag{4}$$

$$\frac{\partial M}{\partial x} = 0 = \frac{\partial I}{\partial x}, \ \frac{\partial T}{\partial x} = 0 \text{ at } x = L_x \tag{5}$$

$$\frac{\partial M}{\partial z} = 0 = \frac{\partial I}{\partial z}, \ \frac{\partial T}{\partial z} = 0 \text{ at } z = 0 \tag{6}$$

$$\frac{\partial M}{\partial z} = 0 = \frac{\partial I}{\partial z}, \; \lambda\frac{\partial T}{\partial z} = -h(T - T_0), \; \text{at } z = L_z \tag{7}$$

where T_0 is the temperature of the monomer−initiator mixture and h is the convective heat transfer coefficient that quantifies the rate of heat transport from the surface to the surrounding. The surface can then be viewed as open to air or as a conducting solid boundary.

In FP experiments, the heat source is removed when the front is observed to propagate. To simulate a finite time of heating, Δt, we can replace the fixed BC eq 4 with a no-flux BC, $(\partial T/\partial x)|_{x=0} = 0$, when $t \geq \Delta t$. We will show below that the results with a constant heat source are recovered when $\Delta t \geq \Delta t_{\min}$, where $\Delta t_{\min}$ is the minimum heating time for the front to propagate in a self-sustained manner. Since the results are unchanged, providing this minimal heating time, we use the fixed BC eq 4 for all times in the rest of this work. With the idea to capture generic properties for the effects of dimensionality on non-adiabatic FP with a minimal RD model, one conductive boundary has been assumed. The difference between one versus two conductive boundaries, at both $z = 0$ and $z = L_z$, is expected to be quantitative only, as detailed in the Discussion and Conclusions section.

Dimensionless Governing Equations. To simplify the numerical analysis, we introduce the dimensionless variables as proposed by Heifetz et al.,[21]

$$J = \sqrt{\frac{I}{I_0}}, \; \psi = \frac{M_0 - M}{M_0}, \; \theta = \frac{T - T_s}{\beta_s T_s}, \; x' = \frac{x}{L_c}, \; z'$$
$$= \frac{z}{L_c}, \; t' = \frac{t}{t_c} \tag{8}$$

where J and θ are the dimensionless initiator concentration and temperature, respectively, and ψ is the degree of conversion that changes from zero (pure monomer) to one (pure polymer). We have also introduced the dimensionless inverse of the effective activation energy, $\beta_s = RT_s/E_{\text{eff}}$, and the characteristic length and time scales, respectively, $L_c = \sqrt{\kappa t_c}$ with $\kappa = \lambda/(\rho_0 c_p)$ the thermal diffusivity, and $t_c = e^{1/\beta_s}/(k_{\text{eff}}^0 \sqrt{I_0})$. The dimensionless form of eqs 1−3 therefore reads, dropping the primes,

$$\frac{\partial J}{\partial t} = -DJ \exp\left(\frac{r\theta}{1 + \beta_s\theta}\right) \tag{9}$$

$$\frac{\partial \psi}{\partial t} = (1 - \psi)J \exp\left(\frac{\theta}{1 + \beta_s\theta}\right) \tag{10}$$

$$\frac{\partial \theta}{\partial t} = \nabla^2\theta + \frac{1}{\delta}(1 - \psi)J \exp\left(\frac{\theta}{1 + \beta_s\theta}\right) \tag{11}$$

where $\delta = RT_s^2/(qM_0 E_{\text{eff}})$, $r = E_d/E_{\text{eff}}$, and $D = k_d(T_s)/(2k_{\text{eff}}(T_s)\sqrt{I_0})$ are the dimensionless forms of the reaction enthalpy, the decomposition activation energy, and the decomposition rate constant at the fixed temperature T_s, respectively.

The initial conditions become, $J(x, z, t = 0) = 1$, $\psi(x, z, t = 0) = 0$, $\theta(x, z, t = 0) \equiv \theta_0 = (T_0 - T_s)/\beta_s T_s$, and the boundary conditions eqs 4−7 write in terms of dimensionless variables, dropping the primes

$$\frac{\partial \psi}{\partial x} = 0 = \frac{\partial J}{\partial x}, \; \theta = 0 \text{ at } x = 0 \tag{12}$$

$$\frac{\partial \psi}{\partial x} = 0 = \frac{\partial J}{\partial x}, \; \frac{\partial \theta}{\partial x} = 0 \text{ at } x = L_x \tag{13}$$

$$\frac{\partial \psi}{\partial z} = 0 = \frac{\partial J}{\partial z}, \; \frac{\partial \theta}{\partial z} = 0 \text{ at } z = 0 \tag{14}$$

$$\frac{\partial \psi}{\partial z} = 0 = \frac{\partial J}{\partial z}, \; \frac{\partial \theta}{\partial z} = -Bi(\theta - \theta_0), \; \text{at } z = L_z \tag{15}$$

where $Bi = hL_c/\lambda$ is the Biot number, which can be seen as the dimensionless form of the convective heat transfer coefficient, h, and thus quantifies the rate of heat loss from the surface to the environment.

Equations 9−15 are numerically integrated using finite-difference and Runge−Kutta fourth-order methods to discretize the spatial and temporal partial derivatives, respectively, where $dz = 0.1$, $dx = 0.05$, and $dt = 5 \times 10^{-5}$ are the typical spatial and temporal step sizes, respectively. Unless otherwise mentioned, the numerical solutions presented hereafter are shown for parameter values in the range of experimental values for FP,[21] here chosen to be $\theta_0 = -7$, $D = 2$, $r = 2$, $\beta_s = 0.09$, and $\delta = 0.05$.

■ RESULTS AND DISCUSSION

Frontal Polymerization in the One-Dimensional Limit. Analytical solutions are readily obtained from eqs 1−3 in the one-dimensional limit, when $L_z \to 0$. Such a limit allows us to derive 1D RD equations similar to the ones used in most FP models[18−20] so that we can highlight the fundamental differences between 1D and 2D nonadiabatic models.

We first average eqs 9−11, along the depth over the interval $[0, L_z]$, and obtain

$$\frac{\partial \langle J \rangle}{\partial t} = -D\left\langle J \exp\left(\frac{r\theta}{1 + \beta_s\theta}\right)\right\rangle \tag{16}$$

$$\frac{\partial \langle \psi \rangle}{\partial t} = -\left\langle (1 - \psi)J \exp\left(\frac{\theta}{1 + \beta_s\theta}\right)\right\rangle \tag{17}$$

$$\frac{\partial \langle \theta \rangle}{\partial t} = \frac{\partial^2 \langle \theta \rangle}{\partial x^2} - \frac{Bi}{L_z}[\theta(x, L_z, t) - \theta_0]$$
$$+ \frac{1}{\delta}\left\langle (1 - \psi)J \exp\left(\frac{\theta}{1 + \beta_s\theta}\right)\right\rangle \tag{18}$$

The depth-averaged quantities are defined as,

$$\langle f \rangle(x, t) = \frac{1}{L_z}\int_0^{L_z} f(x, z, t)dz \tag{19}$$

where f stands for the considered scalar field. We then take the asymptotic limit of small layer thickness, $L_z \to 0$, of eqs 16−18, to obtain the following set of closed 1D equations,

$$\frac{\partial J}{\partial t} = -DJ \exp\left(\frac{r\theta}{1 + \beta_s\theta}\right) \tag{20}$$

$$\frac{\partial \psi}{\partial t} = (1 - \psi)J \exp\left(\frac{\theta}{1 + \beta_s\theta}\right) \tag{21}$$
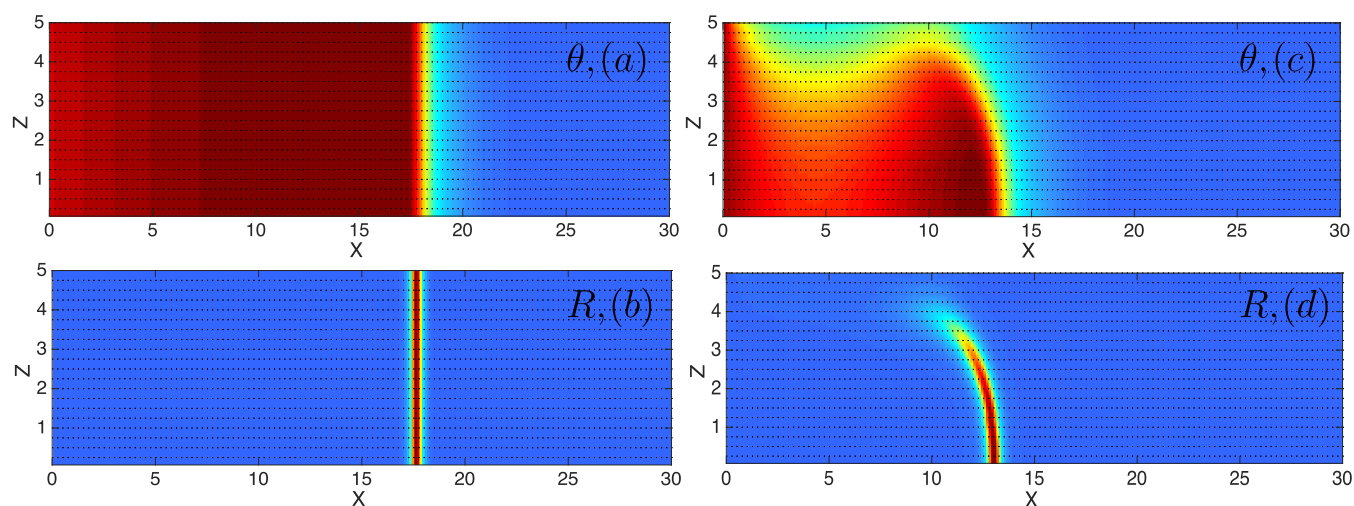
Figure 2. 2D plots of the temperature θ and the reaction rate R in the absence ($Bi = 0$) [(a), (b)] and in the presence [(c), (d)] of heat losses ($Bi = 0.60$), at time $t = 20$, when $L_z = 5$. The numerical values range between (a) $\theta \in [-7, 0.62]$, (b) $R \in [0, 0.63]$, (c) $\theta \in [-7, 0.22]$, (d) $R \in [0, 0.43]$, where the minimum is shown in blue and the maximum in dark red. In the absence of heat losses, the chemical front is planar and separates the hot polymer region from the cold monomer–initiator side. The presence of heat losses deforms the temperature and chemical front across the layer.
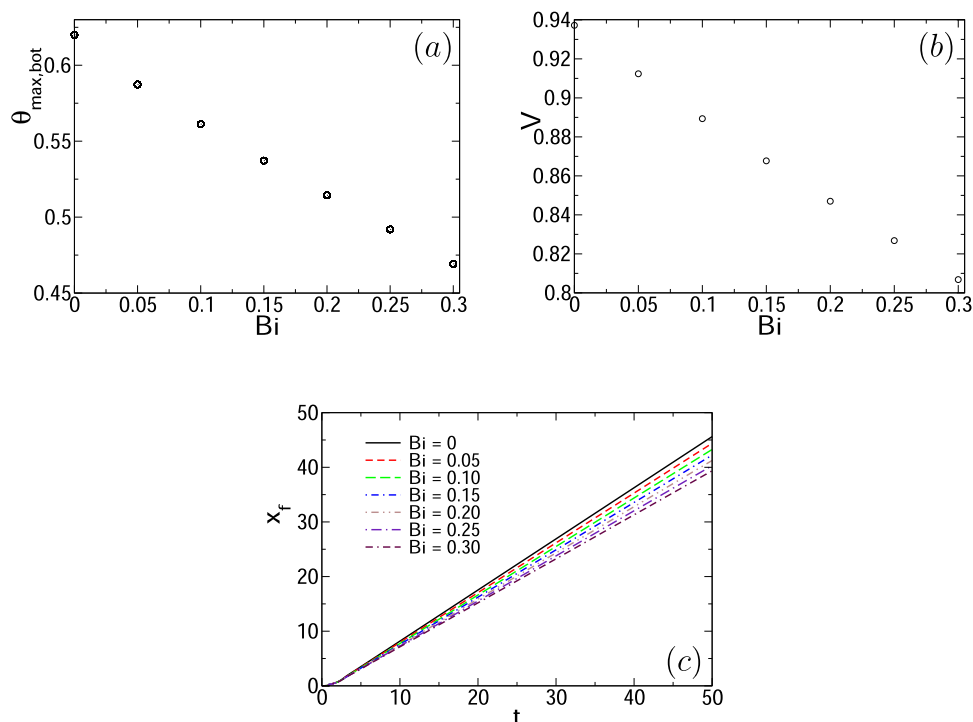

Figure 3. (a) Maximum stationary temperature at the bottom of the system, $\theta_{\mathrm{max,bot}}$, (b) stationary front speed V, and (c) front trajectories $x_f(t)$, for different values of Bi, when $L_z = 5$. As Bi increases, the maximum temperature decreases, which reduces the front speed so that the front travels less far away in the system.

$$\frac{\partial \theta}{\partial t} = \frac{\partial^2 \theta}{\partial x^2} - \alpha(\theta - \theta_0) + \frac{1}{\delta}(1 - \psi)J \exp\left(\frac{\theta}{1 + \beta_s \theta}\right)$$

(22)

where, according to the mean value theorem, $\lim_{L_z \to 0} \langle f \rangle = f(x, 0, t) \equiv f(x,t)$. With eqs 20–22, we recover the 1D model considered by Heifetz et al.[21] to study the effect of heat losses on the front dynamics, with the exception that, in the process of dimensionality reduction, we have been able to explicitly express the dimensionless effective heat loss coefficient, $\alpha =$ Bi/L_z, in eq 22 as a function of the Biot number and the layer thickness.

Although we will integrate the complete model eqs 9–11 numerically in the next section, it is convenient to simplify eqs 20–22 to make the analytical solutions more simple.[18,20] To do so, it is assumed that an appreciable amount of the initiator is consumed in the wake of the moving front and thus, we can neglect the effects of variation of the initiator concentration on the front dynamics. Such a simplification can formally be achieved if we take for instance the limit $D \to 0$ so that the initiator concentration remains constant, $J = 1$, and eq 20 can be
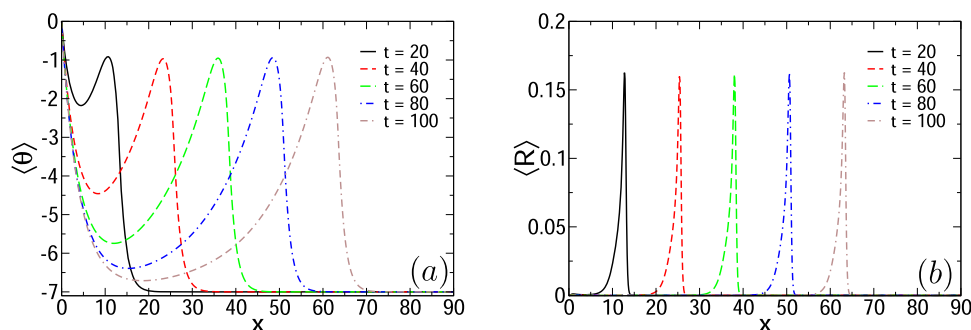
Figure 4. Depth-averaged (a) temperature and (b) reaction rate in the presence of heat losses ($Bi = 0.60 < Bi_{ext}$). A hot spot (local maximum of the temperature) propagates in the system in the course of time with a spatially localized reaction zone.
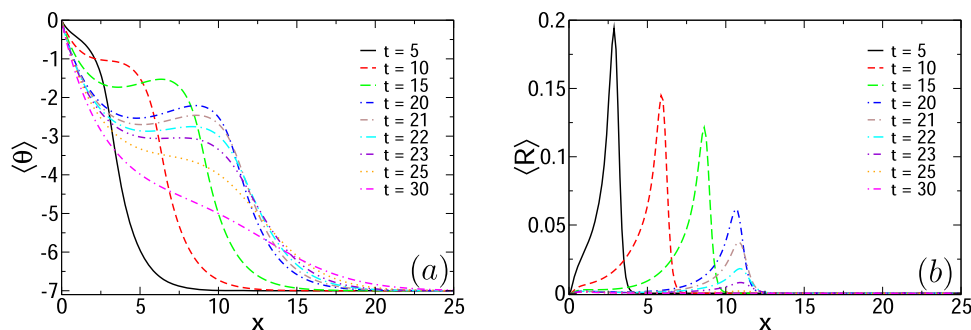

Figure 5. Depth-averaged (a) temperature, and (b) reaction rate in the presence of heat losses ($Bi = 0.80 > Bi_{ext}$). Temperature profiles become monotonous as the reaction rate amplitude reduces over time. Eventually, the front propagation stops with a vanishing reaction rate, $\langle R \rangle \to 0$. In this case, the front dynamics is dominated by heat losses leading to front extinction.

neglected. Equations 20−22 therefore reduce to the so-called one-step FP kinetic model,[18,20]

$$\frac{\partial \psi}{\partial t} = (1 - \psi) \exp\left(\frac{\theta}{1 + \beta_s \theta}\right) \tag{23}$$

$$\frac{\partial \theta}{\partial t} = \frac{\partial^2 \theta}{\partial x^2} - \alpha(\theta - \theta_0) + \frac{1}{\delta}(1 - \psi)\exp\left(\frac{\theta}{1 + \beta_s \theta}\right) \tag{24}$$

It is important to note that no qualitative information is lost by considering the one-step model (eqs 23 and 24), instead of the three-step one (eqs 20−22).[18,20]

The asymptotic analysis of eqs 23 and 24 with the mentioned BCs showed that front extinction always occurs in the long-time limit when $\alpha > \alpha_{ext}$, where $\alpha_{ext} = \frac{t_c V_a^2}{\kappa} \frac{R T_a^2}{2 e E_{eff}(T_a - T_0)}$ in the corresponding one-step model, for large values of the Zeldovich number, $Z = \frac{E_{eff}(T_a - T_0)}{R T_a^2}$, where $T_a = T_0 + q M_0$ and $V_a = \frac{\kappa k_0 R T_a^2}{M_0 q E_{eff}} \exp\left(-\frac{E_{eff}}{R T_a}\right)$ are, respectively, the adiabatic temperature and front speed at the steady state.[18,20] Since $\alpha = Bi/L_z$, we deduce a linear scaling between the Biot number and the layer thickness at the extinction limit defined by the equation $\alpha = \alpha_{ext}$; i.e., $(Bi \sim L_z)_{ext}$. This linear scaling indicates that any modulation of heat losses can exactly be balanced by the same variation of the layer thickness in the asymptotic limit of infinitely small layer thickness. This result is a pure signature of 1D FP models as 2D numerical simulations of eqs 9−11 will demonstrate a strong departure from such a linear regime when the layer thickness is progressively increased (cf. Critical Layer Thickness for Frontal Survival section).

Nonadiabatic Frontal Polymerization in Two Dimensions. *Effects of Heat Losses on FP and Front Extinction.* For $Bi = 0$, the solutions of eqs 9−15 are translationally invariant in the z-direction and thus, $\langle f \rangle(x, t) = f(x, z, t)$, $\forall z$. In the presence of heat losses ($Bi \neq 0$), such a translational invariance is broken and the solutions become z-dependent, as shown in Figure 2, where we compare 2D plots of the temperature and the reaction rate in the absence (Figure 2a,b) and in the presence (Figure 2c,d) of heat losses. In the absence of heat losses, a planar chemical front separates the hot polymer region from the cold monomer−initiator side. The presence of heat losses deforms the temperature and chemical front across the layer. The wavy shape of the contour of the temperature field in Figure 2c is due to the fact that heat losses are stronger in the spatial region between the left system boundary (located at $x = 0$), where the constant heat source is applied, and the position x_f of the localized reaction zone where heat is released (around $x_f = 12.5$ in Figure 2d). Moreover, we note that the maximum reaction rate and temperature are located at the bottom of the system, at $z = 0$, far from the surface from which heat losses occur (see the location of the dark red regions in Figure 2c,d).

We have studied the influence of Bi quantifying the heat losses on the maximum steady temperature at the bottom of the system and on the steady front speed and the front trajectory (see Figure 3). As heat losses increase, the maximum temperature decreases, and the chemical front slows down. We recover here the analytical solutions of the 1D RD model eqs 23 and 24, predicting that the stationary nonadiabatic temperature T_b decreases with increasing the effective heat loss coefficient α.[20] Numerically, we find that the time for the front speed to converge to its steady value is essentially constant, which is noted to be around $t = 10$, in the range of Bi of Figure 3, that we have restricted here below $Bi = 0.30$ due to the presence of

thermal instabilities when $Bi > 0.30$ (cf: Influence of Dimensionality on Thermal Instabilities section).

A particularly important limiting aspect of FP applications is the possibility of front extinction that occurs when heat losses exceed a critical value or equivalently, when $Bi > Bi_{ext}$. We illustrate the survival and extinction of the front numerically in Figures 4 and 5, respectively, when $L_z = 5$. For this value of the layer thickness, we find numerically that $Bi_{ext} = 0.65 \pm 0.05$. When $Bi \leq Bi_{ext}$, a hot spot propagates in the system due to the heat released in the localized reaction zone (see Figure 4a). As discussed below, this propagation does not necessarily occur at a constant speed. The wavy shape in the temperature field observed in Figure 2c translates into a nonmonotonous depth-averaged temperature profile where the sign of the temperature gradient changes twice. Heat diffusion leads to the formation of a polymerization front that travels with the hot spot (see Figure 4b). In this case, the front survives in the presence of heat losses. When $Bi > Bi_{ext}$, heat losses dominate the front dynamics and lead to front extinction. In the long times, the temperature profiles behave as diffusive monotonic profiles (see Figure 5a) and the reaction rate is negligible everywhere (see Figure 5b).

A distinct signature of front extinction can be observed in space-time plots of $\theta(x, z = 0, t)$. Since the temperature reaches its maximum value along the depth at $z = 0$, that position is chosen to obtain Figure 6. In the absence of heat losses, far from the influence of the heat source imposed at the left system boundary, we note that the temperature reaches a stationary value behind the moving front (see Figure 6a). In the presence of heat losses, in contrast to the adiabatic case, the temperature is reduced everywhere behind the moving front (except where it is imposed at the left boundary) (see Figure 6b). When $Bi > Bi_{ext}$ (see Figure 6c), heat losses dominate the front dynamics and lead to front extinction characterized by a comma- or nose-shaped temperature space-time plot.

Critical Layer Thickness for Frontal Survival. 1D FP models are strictly valid in the limit $L_z \rightarrow 0$ only, and the analysis of the front dynamics for arbitrary L_z therefore requires the extension to 2D models.

To demonstrate the antagonistic effect of the layer thickness L_z and the Biot number on the front dynamics, we show the maximum stationary temperature at the bottom of the system ($z = 0$) and the steady front speed for various L_z at fixed Bi (see Figure 7). Increasing the layer thickness enlarges the distance separating the position of the maximum temperature, located at the bottom of the system ($z = 0$), from the surface where heat losses occur, thereby decreasing their effect on the front dynamics. The maximum temperature therefore increases with L_z (see Figure 7a). It is bounded asymptotically, in the limit $L_z \rightarrow \infty$, by the adiabatic temperature, i.e., the maximum temperature in the absence of heat losses. The temperature rise with L_z leads to a faster front, as can be seen in Figure 7b. The time for the front speed to converge to its steady value is essentially constant, around $t = 10$, in the range of L_z considered, as was already noted for different Bi values.

We expect a strong influence of L_z on the possibility of front extinction discussed in the previous section. In Figure 8, we represent the Biot number above which front extinction occurs, Bi_{ext}, as a function of L_z. In the limit $L_z \rightarrow 0$, we recover a linear scaling between Bi_{ext} and L_z as expected from the analysis of FP in the one-dimensional limit (see above). In this limit, 1D models based on the heat equation, eq 22, become valid and heat losses can indeed be described by a single effective heat loss parameter (α) in every point of a 1D system. Then, the
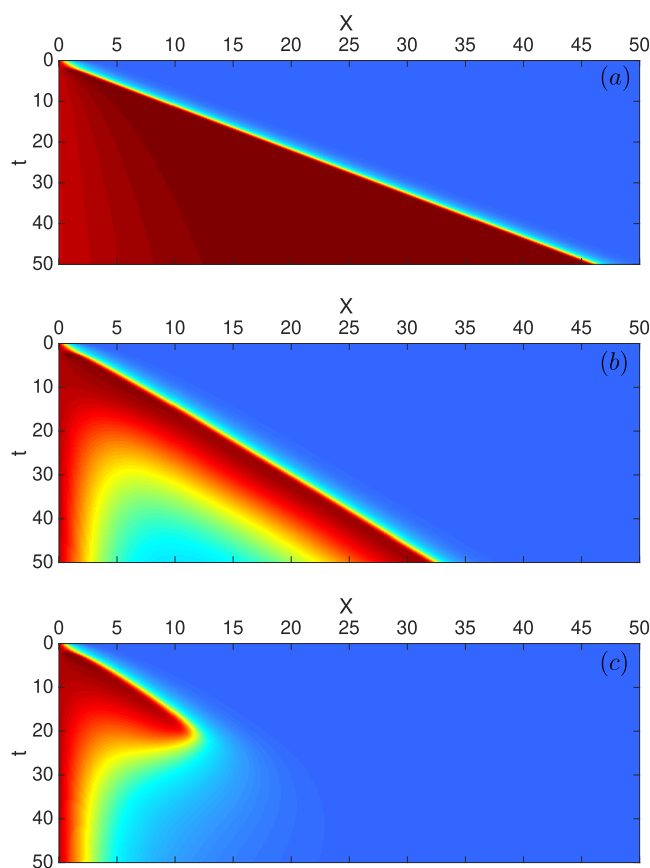

Figure 6. Space-time plots of the temperature field measured at the bottom of the system, $\theta(x, z = 0, t)$, for (a) $Bi = 0$, (b) $Bi = 0.60$, and (c) $Bi = 0.80$, when $L_z = 5$. The numerical values range between (a) $\theta \in [-7, 0.61]$, (b) $\theta \in [-7, 0.47]$ and (c) $\theta \in [-7, 0.45]$, where the minimum (ambient temperature) is shown in blue and the maximum in dark red. The diagonal lines in (a) and (b) express the propagation of the front, while the comma- or nose-like shape in (c) shows the quenching of the front.

condition of front extinction can be rewritten as $\alpha > \alpha_{ext}$, where $\alpha_{ext} = Bi_{ext}/L_z$, and we recover the results for front extinction in 1D provided by Heifetz et al.[21]

However, a strong departure from the linear regime occurs along the extinction limit as a critical extinction point (represented with a cross in Figure 8), for a layer thickness noted $L_{z,cr}$, is approached. When $L_z > L_{z,cr}$, we find that the front propagates independently of Bi, or equivalently, of the heat loss magnitude. In other words, for layers sufficiently thick, it is not possible to stop the front propagation no matter the magnitude of heat losses.

The location of the critical extinction point ($L_{z,cr}$, $Bi_{ext,cr}$) in the (L_z, Bi_{ext}) plane depends on the parameter values. In particular, when δ decreases, more heat is released by the polymerization reaction, thus helping the front to survive. Hence, the extinction limit switches to larger values of Bi_{ext}, and the critical value of the layer thickness decreases, as observed in Figure 8. As δ decreases, the linear regime of the extinction curve is therefore reduced to a smaller range of values of L_z. In Table 1, we summarize the effects of varying the model parameters on the critical extinction point, ($L_{z,cr}$, $Bi_{ext,cr}$), and on the adiabatic front speed V_a. We note that V_z and $Bi_{ext,cr}$ behave in the same way, opposite to $L_{z,cr}$. Indeed, when the front speed decreases, the front is more sensitive to heat losses and requires a thicker layer to survive, which decreases $Bi_{ext,cr}$ and increases $L_{z,cr}$.
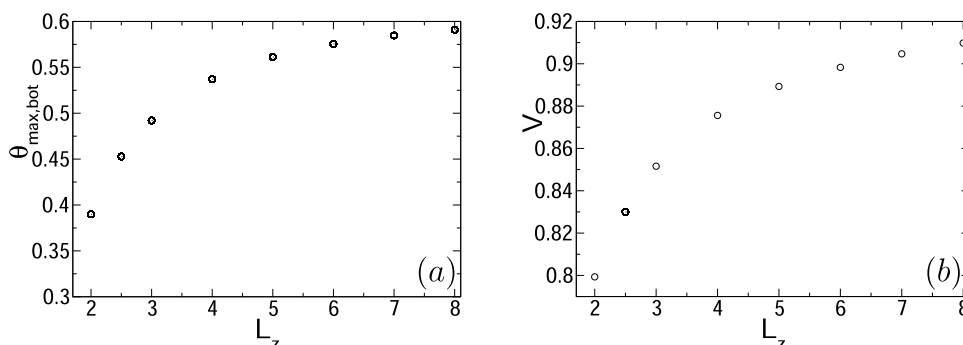
Figure 7. (a) Maximum stationary temperature at the bottom of the system $\theta_{max,bot}$ and (b) stationary front speed V, for different values of L_z, when $Bi = 0.10$. As L_z increases, the maximum stationary temperature and front speed increase. In the limit $L_z \to \infty$, temperature and front speed converge to their corresponding adiabatic value.

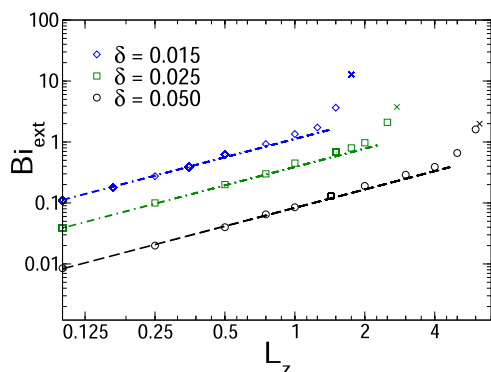**Figure 8.** Plot of Bi_{ext}, the Biot number above which extinction occurs, as a function of L_z, for different values of δ. The straight lines show the linear scalings of Bi_{ext} with L_z, i.e., $Bi_{ext} \sim L_z$. Each extinction limit ends at a critical point (represented with a cross) with abscissa, $L_{z,cr}$. When $L_z > L_{z,cr}$, the front survives independently of the heat loss magnitude. The values $Bi_{ext} \pm \Delta Bi_{ext}$ and $L_{z,cr} \pm \Delta L_{z,cr}$ are numerically calculated with maximum uncertainties of $\Delta Bi_{ext} = 0.05$ and $\Delta L_{z,cr} = 0.25$.

Table 1. Relations between the Critical Extinction Point $(L_{z,cr}, Bi_{ext,cr})$ and Adiabatic Front Speed V_a with the Model Parameters $(D, \delta, \beta_s, r, \theta_0)$ Involved in the Three-Step FP Model[a]

model parameters	definitions	$L_{z,cr}$	$Bi_{ext,cr}$	V_a
D	$k_d(T_s)/(2k_{eff}(T_s)\sqrt{I_0})$	+	−	−
δ	$RT_s^2/(qM_0E_{eff})$	+	−	−
β_s	RT_s/E_{eff}	−	+	+
r	E_d/E_{eff}	−	+	+
θ_0	$(T_0 - T_s)/\beta_s T_s$	−	+	+

[a]A positive (or negative) sign means that, when the parameter increases, the variable increases (or decreases). Unless the parameters are varied, the table is numerically obtained when the above-mentioned set of parameters is (2, 0.05, 0.09, 2, −7).

The passage from a linear to a nonlinear scaling law between Bi_{ext} and L_z highlights the fundamental difference between 1D and 2D solutions based on eqs 20−22 and eqs 9−11, respectively. In the 1D view of FP, heat losses are described by the effective parameter, $\alpha = Bi/L_z$. This means that any scaling of the layer thickness, aL_z, with constant $a > 0$, and of the Biot number, aBi, leaves the front dynamics unchanged. The 1D picture therefore suggests that the increase in heat produced with the layer thickness can exactly be balanced by the same increase in heat losses.

Departure from Linear Relationship. For 2D systems, such a picture does not hold. To understand the failure of the 1D predictions, the maximum stationary temperature at the bottom of the system ($z = 0$) is measured for some couples of points $(aL_{z,1}; aBi_1)$, with $a > 0$ (see Figure 9). We note that it increases
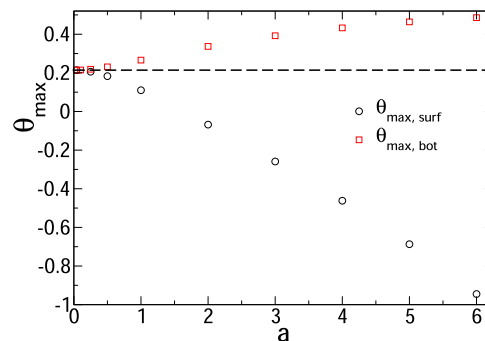

Figure 9. Maximum stationary temperature measured at the bottom of the system (global maximum), $\theta_{max,bot}$ (squares), and at the surface (circles) (local maximum), $\theta_{max,surf}$ for couples of points ($L_z = aL_{z,1}$; $Bi = aBi_1$), with $L_{z,1} = 1$ and $Bi_1 = 0.06$, and $a > 0$. The maximum temperature increases with a at the bottom, while the opposite situation occurs at the surface of the system. The solution for the temperature based on the 1D RD model (eqs 23 and 24) is recovered when $a \to 0$ or equivalently, when $L_z \to 0$. The 1D model predicts a constant value for the temperature, $\theta_{max,surf} = \theta_{max,bot} = \theta_{max}$ $\forall a$ (dashed line).

with a, while the 1D solution predicts a constant value for the temperature, $\forall a$. This is because, in two dimensions, the detailed dynamics of heat losses occurring from the surface can be accounted for. The temperature is therefore larger at the bottom of the system with respect to the 1D solution. Thus, a similar increase in L_z and Bi favors the front survival. In particular, if we increase L_z from an extinction point, a larger increase of Bi is required to recover the extinction limit. However, we note that the linear regime is an excellent approximation over a wide range of values of layer thicknesses $L_z \ll L_{z,cr}$, as observed in Figure 8.

We can proceed to the same analysis by measuring the maximum temperature at the surface (shown as circles in Figure 9). Unlike the maximum temperature at $z = 0$, the surface temperature decreases when a increases. This opposite trend is explained by the stronger sensitivity of the surface to heat losses as can be seen by comparing two characteristic time scales. An increase of L_z reduces the effect of heat losses at the bottom of the system and thus, by continuity, enhances the surface temperature. If we assume that the reaction zone is essentially

located at $z = 0$, the characteristic time for heat to feed the surface by vertical diffusion is proportional to L_z^2. On the other hand, an increase of Bi reduces the surface temperature in a characteristic time proportional to $1/h \sim 1/Bi$, with h the convective heat transfer coefficient. Thus, at the surface, a similar increase of L_z and Bi favors heat losses and the surface temperature decreases with a. As a corollary, as $L_z \rightarrow L_{z,cr}$ along the extinction limit in Figure 8, the surface cools down.

We note that, in the limit $a \rightarrow 0$, the temperature becomes independent of z and converges to the 1D solution of eqs 20–22 (dashed line in Figure 9). Also, as $a \rightarrow \infty$, $\theta_{max,bot}$ and $\theta_{max,surf}$ are bounded, respectively, by the adiabatic and ambient temperatures, respectively.

Existence of Critical Layer Thickness. The cooling of the surface as $L_z \rightarrow L_{z,cr}$ along the extinction limit deeply affects the front dynamics. In particular, the front survival that occurs when $L_z > L_{z,cr}$, $\forall Bi$, imposes a scaling law for the driving force, $\Delta\theta_{surf} = \theta(x, z = L_z, t) - \theta_0$, associated with heat losses. Indeed, from eq 18, that we rewrite here for convenience,

$$\frac{\partial \langle \theta \rangle}{\partial t} = \frac{\partial^2 \langle \theta \rangle}{\partial x^2} - \frac{Bi}{L_z}\Delta\theta_{surf} + \frac{1}{\delta}\left\langle (1 - \psi)J \right.$$

$$\left. \exp\left(\frac{\theta}{1 + \beta_s\theta}\right)\right\rangle \tag{25}$$

we expect the front dynamics to be insensitive to heat losses when the second right-hand-side term is independent of Bi, i.e., when $\Delta\theta_{surf} \sim 1/Bi$. Such a scaling is corroborated numerically in the long-time limit as Bi increases when $L_z > L_{z,cr}$, as illustrated for the maximum of $\Delta\theta_{surf}$ (see Figure 10).
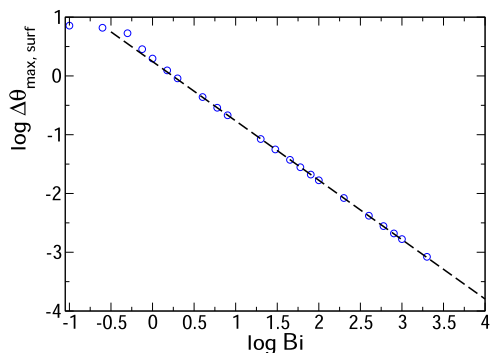

Figure 10. Log–log plot of the difference between the maximum stationary surface temperature and the ambient temperature, $\Delta\theta_{max,surf} = \theta_{max,surf} - \theta_0$, as a function of Bi, when $L_z = 7$, above the critical layer thickness of $L_{z,cr} = 6.25 \pm 0.25$. The dashed line is a straight line whose equation writes $\log \Delta\theta_{max,surf} = 0.25 - 1.0 \times \log Bi$.

The observed scaling of $\Delta\theta_{surf}$ with Bi provides a simple physical interpretation for the existence of such a critical layer thickness. As $Bi \rightarrow \infty$ when $L_z > L_{z,cr}$, the rate at which heat is lost from the surface to the surrounding, which is quantified by Bi (see eq 15), is exactly balanced by the rate at which the surface cools down, $\Delta\theta_{surf} \sim 1/Bi$. In this case, any increase in the rate of heat losses reduces the surface temperature at the same rate leaving eq 25, and therefore the front dynamics, unchanged and the front survives $\forall Bi$.

Effect of Heating Time on Nonadiabatic Frontal Polymerization. Under nonadiabatic conditions, the solutions become z-dependent and the minimum heating time, Δt_{min}, is expected to depend on L_z and $Bi \neq 0$. Our main objective here is to show how such a dependence occurs.

For the sake of comparison with the adiabatic case, we first demonstrate the existence of a minimum heating time, Δt_{min}, in the presence of heat losses in Figure 11. The space-time plots of
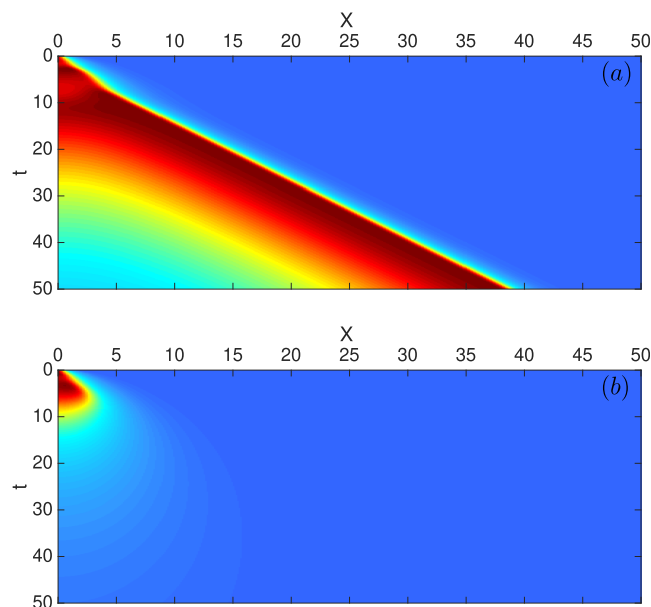

Figure 11. Space-time plots of the temperature field, $\theta(x, z, t)$, at the bottom of the system ($z = 0$) in the presence of heat losses ($Bi = 0.30$) and $L_z = 5$, with a heating time of (a) $\Delta t = 1.40$ and (b) $\Delta t = 1.30$. The numerical values range between (a) $\theta \in [-7, 0.50]$ and (b) $\theta \in [-7, 0]$, where the minimum (the ambient temperature) is shown in blue and the maximum in dark red. For the parameter values considered here, the minimum heating time is $\Delta t_{min} = 1.35(\pm 0.05)$. In (a), $\Delta t \geq \Delta t_{min}$, the front propagates in a self-sustained manner and the temperature decreases in time behind the moving front due to heat losses. In (b), $\Delta t < \Delta t_{min}$, the front is quenched due to an insufficient heating time.

the temperature field are illustrated when $Bi \neq 0$ at the bottom of the system, $z = 0$, where the temperature reaches its maximum value along the depth, when $\Delta t \geq \Delta t_{min}$ and when $\Delta t < \Delta t_{min}$. When $\Delta t \geq \Delta t_{min}$, the front propagates in a self-sustained manner and, in contrast to the adiabatic case, the temperature reduces in time behind the moving front due to the presence of heat losses and converges to the ambient temperature as time evolves. When $\Delta t < \Delta t_{min}$, the front is quenched as a result of an insufficient heating time. In this particular case of study, for which $L_z = 5$ and $Bi = 0.30$, $\Delta t_{min} = 1.35 \pm 0.05$, which is larger than the minimum heating time $\Delta t_{min} = 1.13 \pm 0.13$ obtained in the adiabatic case (see Figure 12).

The presence of heat losses reduces the front speed and temperature so that Δt_{min} increases when Bi increases (see Figure 12a). When $L_z \leq L_{z,cr}$, front extinction due to heat losses occurs when $Bi > Bi_{ext}$ and Δt_{min} reaches a maximum value when $Bi = Bi_{ext}$. We note that, when $L_z > L_{z,cr}$, the front dynamics is insensitive to Bi (large Bi), and so is Δt_{min}. At fixed Bi, increasing the layer thickness favors the front survival, which reduces the time required for front propagation (see Figure 12b). In the limit $L_z \rightarrow \infty$, the temperature and front speed converge to their adiabatic solution, so Δt_{min} is independent of L_z. From Figure 12, we note that the largest variations of Δt_{min} with L_z and Bi are located close to the extinction limit (vertical dotted lines), where
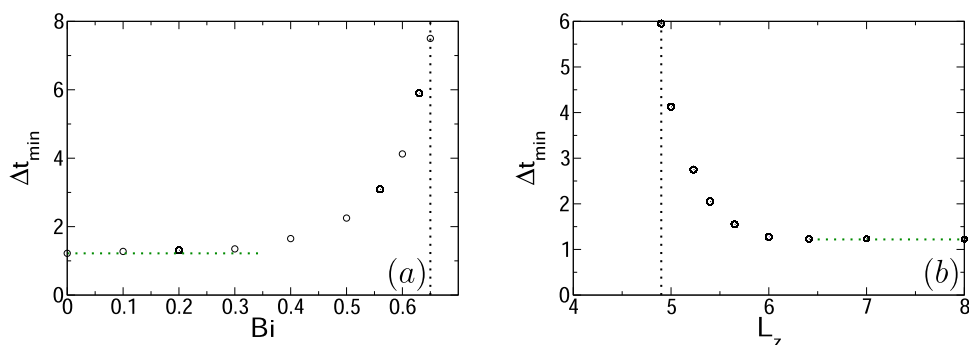
Figure 12. Minimum heating time $\Delta t_{\min}$, as a function of (a) Bi when $L_z = 5$ and (b) L_z when $Bi = 0.60$. The domain in Bi and L_z are limited by the extinction limits (vertical dotted lines). More time of heating is required for a self-sustained front when heat losses increase. As $Bi \to 0$ or $L_z \to \infty$, the minimum heating time converges to the one of an adiabatic front (horizontal dotted line).
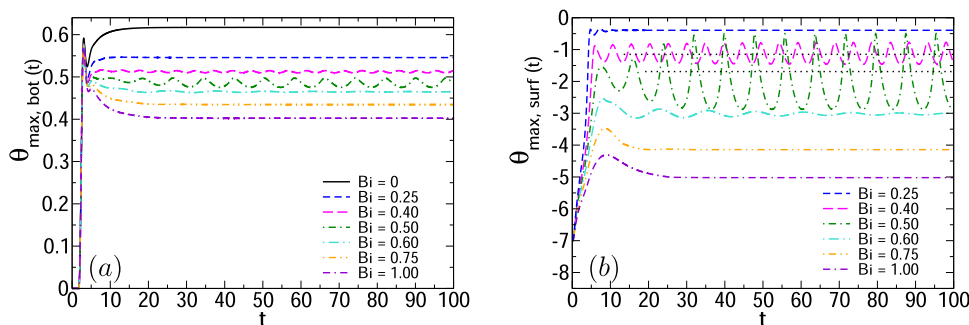

Figure 13. Temporal evolution of the maximum temperature (a) at the bottom of the system $\theta_{\max,\text{bot}}(t)$ (from $x = 0$ to L_x) and (b) at the surface $\theta_{\max,\text{surf}}(t)$ (from $x = 2$ to L_x), for different values of Bi, when $L_z = 7$. Note that we have shifted the initial position of the spatial domain in which the maximum temperature is calculated in (b) since the maximum temperature inside the reaction zone that we seek to follow is smaller than the fixed temperature $\theta = 0$ at $x = 0$ for the considered values of Bi. As Bi increases, the front destabilizes and the maximum temperature oscillates in time. Increasing further Bi leads to a stable front and the maximum temperature reaches a steady value after a transient regime. The dotted lines in (b) are the steady value around which the sustained oscillations occur.
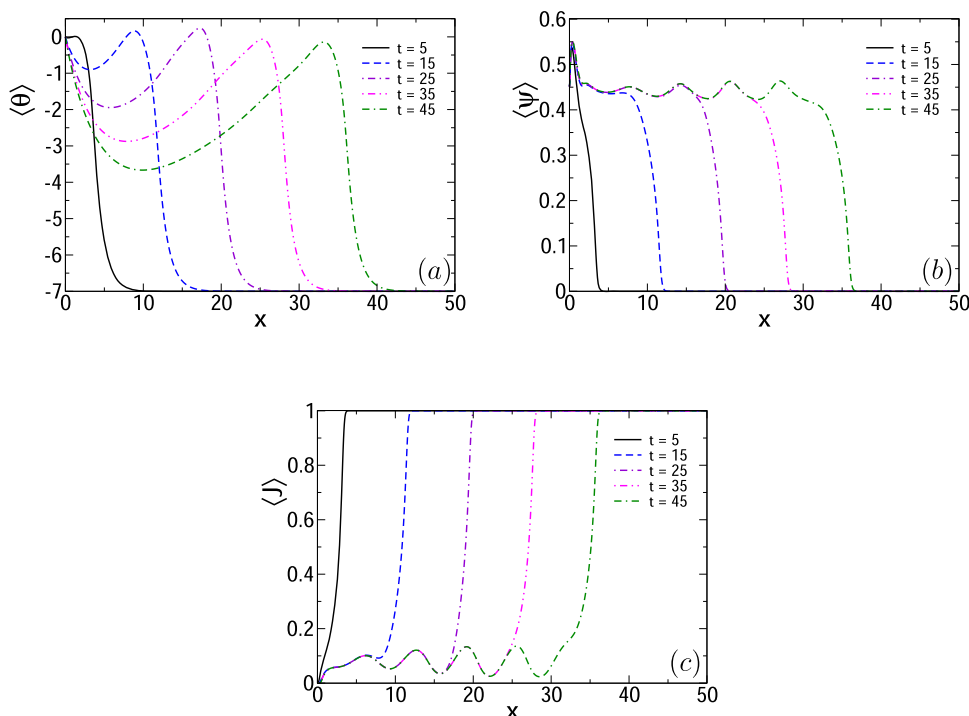

Figure 14. Depth-averaged (a) temperature, (b) degree of conversion, and (c) initiator concentration profiles at different times for $L_z = 7$ and $Bi = 0.50$. Spatial oscillations occur in the degree of conversion and initiator concentration profiles behind the moving front due to thermal instabilities.

the sensitivity to heat losses is the most pronounced, while Δt_{min} is essentially independent of L_z and Bi far from this limit.

For the range of values tested for L_z and Bi, we find that the time to reach the steady state is close but not equal to the maximum value of Δt_{min}. It is typically larger than 10 while the maximum value of Δt_{min} is found to be smaller than 8 (see Figure 12a).

Influence of Dimensionality on Thermal Instabilities. Polymerization fronts do not necessarily travel at a constant speed.[2] In particular, under nonadiabatic conditions, from a linear stability analysis (LSA) of 1D uniformly propagating polymerization fronts, i.e., fronts that propagate with a constant velocity and with steady temperature and degree of conversion behind the moving front, it was shown that the front can lose its stability due to the increase in heat losses to the environment.[20] Here, our main objective is to show how the predictions of thermal instabilities based on 1D models can be affected by the second dimension.

The LSA of 1D fronts[20] shows that when increasing heat losses to the surrounding, the front is slower and remains in or gets closer to the unstable regime. Thus, in 1D systems (associated with the limit, $L_z \rightarrow 0$), it is not possible to stabilize a 1D front by increasing heat losses, i.e., by increasing Bi. In 2D systems, an unstable front can be stabilized by an increase in heat losses. This is shown numerically in the temporal evolution of the maximum temperatures when in particular, $L_z > L_{z,cr}$, as Bi increases (see Figure 13). As shown in Figure 13a, increasing Bi up to $Bi = 0.50$ destabilizes the front and leads to sustained oscillations. Increasing further Bi from $Bi = 0.50$ leads to damped oscillations at $Bi = 0.60$ and no oscillation above $Bi = 0.75$, when a stable front is recovered. We note that this scenario, which can be summarized by the following scheme, "stable front $(Bi = 0) \xrightarrow{Bi}$ unstable front $\xrightarrow{Bi}$ stable front $\xrightarrow{Bi}$ front survival ($\forall Bi$) when $L_z > L_{z,cr}$", is unique to 2D systems. We relate this scheme to the insensitivity of the front dynamics to heat losses when both Bi and L_z are sufficiently large (cf. Critical Layer Thickness for Frontal Survival section).

Thermal instabilities can also be seen at the surface (see Figure 13b). The amplitudes of oscillations are larger at the surface than at the bottom due to the more pronounced sensitivity to heat losses. The frequency of oscillations is however relatively less sensitive to the position across the layer at which the temperature profile is plotted. Further, we note that the large amplitude of temperature oscillations induced by increasing Bi can increase the temperature, at least locally in time, as shown in Figure 13b. However, the stationary values around which the temperature oscillates are shown to decrease with Bi (see dotted lines in Figure 13b). Figure 13 therefore suggests that thermochemical instabilities expand through the whole thickness.

The diffusion of heat added to the variation in time of the temperature inside the reaction zone leads to spatial oscillations of the degree of conversion (or reaction yield) and of the initiator concentrations behind the moving front (see Figure 14).

The influence of layer thickness is shown in Figure 15. For the chosen parameters, when L_z increases, the amplitude and period of oscillations reduce and eventually, as $L_z \rightarrow \infty$, the front becomes stable and we recover the stability of the adiabatic front. In contrast to increasing Bi, we observe numerically in the range of parameters tested that increasing L_z always stabilizes the front as in Figure 15.
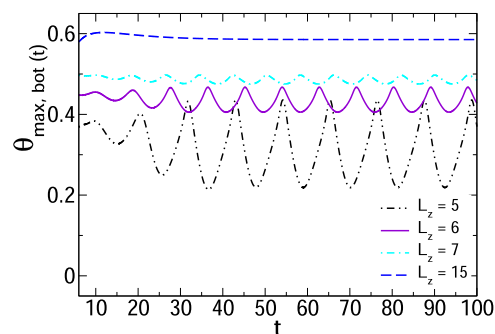

Figure 15. Temporal evolution of the maximum temperature at the bottom of the system $\theta_{max,bot}(t)$ for different values of L_z, when $Bi = 0.50$. Increasing L_z reduces the amplitude and period of oscillations so that temperature reaches a steady-state characteristic of a stable front as $L_z \rightarrow \infty$.

■ DISCUSSION AND CONCLUSIONS

In this work, we have studied analytically and numerically the frontal polymerization (FP) of a monomer−initiator mixture in a 2D system of layer thickness L_z, when heat losses to the surrounding occur at one of the horizontal boundaries. The front is initiated by a constant heat source applied at one of the lateral boundaries that is shown not to affect the system dynamics after a minimal time of heating. The model of FP rests on the heat equation and the kinetic equations describing the spatio-temporal evolution of the temperature and of the monomer and initiator concentrations, respectively. In the limit $L_z \rightarrow 0$, we have first recovered the predictions of 1D models that encode heat losses in an effective heat loss parameter $\alpha = Bi/L_z$ in the heat equation. As a signature of 1D models, it is shown analytically that a linear dependence exists between Bi (quantifying the rate of heat loss to the surrounding) and L_z at the extinction limit, i.e., $Bi_{ext} \sim L_z$. A failure of such a linear scaling, and of 1D predictions, is demonstrated as the layer thickness is progressively increased in the numerical integration of the 2D model. In particular, a strong deviation from the linear regime is observed close to the critical value of the layer thickness, $L_{z,cr}$, above which the front survives independently of heat losses. The approach toward the criticality manifests itself in the form of a scaling law for the driving force associated with heat losses, $\Delta\theta_{surf} = (\theta_{surf} - \theta_0) \sim 1/Bi$, valid when $L_z > L_{z,cr}$ as $Bi \rightarrow \infty$, and where θ_{surf} is the dimensionless surface temperature. In this case, any increase in the rate of heat losses reduces the surface temperature at the same rate so that the front survives independently of heat losses.

Furthermore, we have shown that the second dimension brings new thermal instabilities scenarios compared to 1D models. The latter predict no possibility of stabilization of a front by increasing heat losses. Based on 2D models, we found that the front may be stabilized by increasing Bi. In the range of parameter values tested, we have also seen that increasing L_z always makes the front more stable by decreasing the amplitude of oscillations.

Combustion fronts are classical examples of self-sustained reaction fronts whose properties are well known to share similarities with FP (see ref 18 and references therein). Such fronts have been extensively studied in rectilinear and cylindrical geometries with a particular focus on the steady state and its stability.[29−34] In particular, with heat losses, combustion fronts are similarly characterized by a strong deformation of the reaction zone and by the presence of an essentially nonreactive

layer near the boundaries when heat losses are important.[29−31] Such heat losses also affect the stability boundaries of the stationary combustion front and the reaction yield.[29,32−34] The similarity between thermal polymerization and combustion fronts suggests that the present results of the effects of dimensionality on the front dynamics and stability could also be of great relevance to combustion problems. More extensive studies are required to check the latter statement.

In terms of dimensional variables, if we use typical orders of magnitude for parameter values in FP (see Table 2), we obtain β_s

Table 2. Typical Order of Magnitude for the Dimensional Model Parameters in Experiments of Frontal Polymerization[14,19,20]

model parameters	values	units
I_0, M_0	0.10, 10	mol/L
κ	0.0010	cm^2/s
k_{eff}^0	1.0×10^9	L$^{1/2}$/(s·mol$^{1/2}$)
T_0, T_s	300, 500	K
q	35	L·K/mol
E_{eff}	100	kJ/mol

$\equiv RT_s/E_{eff} = 0.042$ and $\delta = 0.059$. We then obtain a characteristic length scale of $L_c = \sqrt{\kappa t_c} = 0.30$ cm, where $t_c = e^{1/\beta_s}/(k_{eff}^0 \sqrt{I_0})$. In this case, we numerically found $L'_{z,cr} = L_{z,cr}/L_c \simeq 20$, where we have reintroduced for this paragraph the prime notation for dimensionless space variables to differentiate with the dimensional layer thickness. Hence, we obtain for the latter the value of $L_{z,cr} = 6.0$ cm, which is in the range of experimental values of interest for FP. We note that the (dimensional) critical layer thickness can a priori easily be controlled experimentally by varying the initial initiator concentration, I_0. The dependence of dimensional quantities on I_0 also provides a relatively simple way to check the linear scaling obtained in the 1D limit at the extinction limit. Indeed, since $L'_z \sim Bi_{ext}$, the dimensional layer thickness scales as $L_z \sim L_{c,ext}^2$ or equivalently as $L_z \sim I_{0,ext}^{-1/2}$, where we recall that $Bi = hL_c/\lambda$. An experimental setup similar to the one used by Bansal et al.[25] could be used to verify this scaling law.

The results obtained in this work could provide a first step toward the control strategy and the design of FP in thin layers. Some extensions of this work are envisioned. First, we could consider two conductive horizontal boundaries instead of one. In that case, the insulated boundary condition at the system bottom of eq 6 is replaced by $\lambda(\partial T/\partial z)|_{z=0} = h_{bot}(T|_{z=0} - T_0)$, where h_{bot} is the convective heat loss coefficient that quantifies the rate at which heat losses occur from the system bottom boundary. We have checked numerically that, in that case, we can draw a similar extinction curve in the (Bi_{ext}, L_z) plane as in Figure 8. In the presence of two conductive boundaries, the front is more sensitive to heat losses so that each extinction limit in Figure 8 is shifted to smaller values of Bi_{ext} and larger values of $L_{z,cr}$ at fixed Bi_{bot}, where $Bi_{bot} = h_{bot}L_c/\lambda$, and Bi_{ext} has the same definition as before and relates to the surface. The shifting of the extinction limit can be shown analytically in the 1D limit. Indeed, as $L_z \to 0$, the same strategy can be applied to obtain an equation similar to eq 24, i.e.,

$$\partial\theta/\partial t \sim -\alpha_2(\theta - \theta_0) \text{ where } \alpha_2 = (Bi_{surf} + Bi_{bot})/L_z$$
(24b)

with $Bi_{surf} = hL_c/\lambda$. Thus, in the 1D limit, heat losses are additive. Since eq 24 and eq 24b have an identical form, the general

solutions of the nonadiabatic problem[20] are unchanged. In particular, at the extinction limit, α and α_2 have the same value, and therefore the Biot numbers at the extinction limit are related to each other by the relation Bi (one conductive boundary) = $Bi_{surf} + Bi_{bot}$, where the term on the left-hand side is the Biot number when there is one (surface or bottom) conductive element. In particular, when varying only the surface Biot number Bi_{surf} while keeping Bi_{bot} fixed, we obtain at the extinction limit that Bi_{ext} (two conductive boundaries) = Bi_{ext} (one conductive boundary) − Bi_{bot} so that each value of Bi_{ext} in Figure 8 is decreased by a quantity exactly equal to Bi_{bot} as $L_z \to 0$. As expected, we also deduce that it is always easier to quench a front when there is two conductive boundaries. As the layer thickness progressively increases close to its critical value, eq 24b becomes invalid, which violates the additivity property of heat losses.

Next, a full classification of thermal instabilities and their nature in the (L_z, Bi) plane could be of interest for the control and design of new materials based on such instabilities.[24,35,36] Finally, in this work, we have also assumed an infinitely large viscosity of the monomer−initiator mixture to prevent any convective motion. In a subsequent work, we will investigate the influence of natural convection on the dynamics of a polymerization front traveling perpendicularly to the gravity field in the more general framework of reaction−diffusion−convection models.

■ AUTHOR INFORMATION

Corresponding Authors
Reda Tiani − *Nonlinear Physical Chemistry Unit, Université libre de Bruxelles (ULB), Faculté des Sciences, CP231, 1050 Brussels, Belgium;* ● orcid.org/0000-0002-4070-565X; Email: reda.tiani@ulb.be

Laurence Rongy − *Nonlinear Physical Chemistry Unit, Université libre de Bruxelles (ULB), Faculté des Sciences, CP231, 1050 Brussels, Belgium;* ● orcid.org/0000-0002-3556-7045; Email: laurence.rongy@ulb.be

Author
John A. Pojman − *Department of Chemistry, Louisiana State University, Baton Rouge, Louisiana 70803, United States;* ● orcid.org/0000-0003-4788-8767

Complete contact information is available at:
https://pubs.acs.org/10.1021/acs.jpcb.2c01252

Notes
The authors declare no competing financial interest.

■ ACKNOWLEDGMENTS

■ REFERENCES

(1) Pojman, J. A.; Qui, T.-C.-M. *Nonlinear Dynamics with Polymers: Fundamentals, Methods and Applications*, 1st ed.; Wiley-VCH Verlag GmbH & Co. KGaA: Weinheim, Germany, 2010.

(2) Pojman, J. A. *Polymer Science: A Comprehensive Reference*, 1st ed.; Elsevier: Amsterdam, 2012.

(3) Goli, E.; Robertson, I. D.; Geubelle, P. H.; Moore, J. S. Frontal Polymerization of Dicyclopentadiene: A Numerical Study. *J. Phys. Chem. B* **2018**, *122*, 4583−4591.

(4) Chen, S.; Sui, J.; Chen, L.; Pojman, J. A. Polyurethane-Nanosilica Hybrid Nanocomposites Synthesized by Frontal Polymerization. *J. Polym. Sci., Part A: Polym. Chem.* **2005**, *43*, 1670−1680.

(5) Mariani, A.; Alzari, V.; Monticelli, O.; Pojman, J. A.; Caria, G. Polymeric Nanocomposites Containing Polyhedral Oligomeric Silsesquioxanes (Poss) Prepared Via Frontal Polymerization. *J. Polym. Sci., Part A: Polym. Chem.* **2007**, *45*, 4514−4521.

(6) Yan, Q.-Z.; Zhang, W.-F.; Lu, G.-D.; Su, X.-T.; Ge, C.-C. Frontal Polymerization Synthesis of Starch-Grafted Hydrogels: Effect of Temperature and Tube Size on Propagating Front and Properties of Hydrogels. *Chem. - Eur. J.* **2006**, *12*, 3303−3309.

(7) Guo, X.; Wang, C.-F.; Fang, Y.; Chen, L.; Chen, S. Fast Synthesis of Versatile Nanocrystal-Embedded Hydrogels toward the Sensingof Heavy Metal Ions and Organoamines. *J. Mater. Chem.* **2011**, *21*, 1124−1129.

(8) Sanna, R.; Alzari, V.; Nuvoli, D.; Scognamillo, S.; Marceddu, S.; Mariani, A. Polymer Hydrogels of 2-Hydroxyethyl Acrylate and Acrylic Acid Obtained by Frontal Polymerization. *J. Polym. Sci., Part A: Polym. Chem.* **2012**, *50*, 1515−1520.

(9) Nagy, I. P.; Sike, L.; Pojman, J. A. Thermochromic Composite Prepared Via a Propagating Polymerization Front. *J. Am. Chem. Soc.* **1995**, *117*, 3611−3612.

(10) He, M.; Huang, X.; Zeng, Z.; Yang, J. Photo-triggered redox frontal polymerization: A new tool for synthesizing thermally sensitive materials. *J. Polym. Sci., Part A: Polym. Chem.* **2013**, *51*, 4515−4521.

(11) Robertson, I. D.; Yourdkhani, M.; Centellas, P. J.; Aw, J. E.; Ivanoff, D. G.; Goli, E.; Lloyd, E. M.; Dean, L. M.; Sottos, N. R.; Geubelle, P. H.; et al. Rapid energy-efficient manufacturing of polymers and composites via frontal polymerization. *Nature* **2018**, *557*, 223−227.

(12) White, S. R.; Kim, C. A Simultaneous Lay-Up and in situ Cure Process for Thick Composites. *J. Reinf. Plast. Compos.* **1993**, *12*, 520−535.

(13) Sangermano, M.; Antonazzo, I.; Sisca, L.; Carello, M. Photoinduced cationic frontal polymerization of epoxy-carbon fibre composites. *Polym. Int.* **2019**, *68*, 1662−1665.

(14) Goldfeder, P. M.; Volpert, V. A.; Ilyashenko, V. M.; Khan, A. M.; Pojman, J. A.; Solovyov, S. E. Mathematical Modeling of Free-Radical Polymerization Fronts. *J. Phys. Chem. B* **1997**, *101*, 3474−3482.

(15) Schult, D. A.; Volpert, V. A. Linear Stability Analysis of Thermal Free Radical Polymerization Waves. *Int. J. Self-Propag. High-Temp. Synth.* **1999**, *8*, 417−440.

(16) Gross, L. K.; Volpert, V. A. Weakly Nonlinear Stability Analysis of Frontal Polymerization. *Stud. Appl. Math.* **2003**, *110*, 351−375.

(17) Cardarelli, S. A.; Golovaty, D.; Gross, L.; Gyrya, V. T.; Zhu, J. A Numerical Study of One-step Models of Polymerization: Frontal versus Bulk Mode. *Phys. D* **2005**, *206*, 145−165.

(18) Volpert, V. A. *Self-Assembly, Pattern Formation and Growth Phenomena in Nano-Systems*, 1st ed.; Springer: Dordrecht, 2006.

(19) Goldfeder, P. M.; Volpert, V. A. Nonadiabatic frontal polymerization. *J. Eng. Math.* **1998**, *34*, 301−318.

(20) Spade, C. A.; Volpert, V. A. Linear Stability Analysis of Nonadiabatic Free Radical Polymerization Waves. *Combust. Theory Model.* **2001**, *5*, 21−29.

(21) Heifetz, A.; Ritter, L. R.; Olmstead, W. E.; Volpert, V. A. A Numerical Analysis of Initiation of Polymerization Waves. *Math. Comput. Model.* **2005**, *41*, 271−285.

(22) Comissiong, D. M. G.; Gross, L. K.; Volpert, V. A. Frontal Polymerization in the Presence of an Inert Material. *J. Eng. Math.* **2006**, *54*, 389−402.

(23) Comissiong, D. M. G.; Gross, L. K.; Volpert, V. A. The Enhancement of Weakly Exothermic Polymerization Fronts. *J. Eng. Math.* **2007**, *57*, 423−435.

(24) Goli, E.; Peterson, S. R.; Geubelle, P. H. Instabilities driven by frontal polymerization in thermosetting polymers and composites. *Composites, Part B* **2020**, *199*, No. 108306.

(25) Bansal, K.; Pojman, J. A.; Webster, D.; Quadir, M. Frontal Polymerization of a Thin Film on a Wood Substrate. *ACS Macro Lett.* **2020**, *9*, 169−173.

(26) Goli, E.; Robertson, I. D.; Agarwal, H.; Pruitt, E. L.; Grolman, J. M.; Geubelle, P. H.; Moore, J. S. Frontal polymerization accelerated by continuous conductive elements. *J. Appl. Polym. Sci.* **2019**, *136*, No. 47418.

(27) Frulloni, E.; Salinas, M. M.; Torre, L.; Mariani, A.; Kenny, J. M. Numerical Modeling and Experimental Study of the Frontal Polymerization of the Diglycidyl Ether of Bisphenol a/Diethylenetriamine Epoxy System. *J. Appl. Polym. Sci.* **2005**, *96*, 1756−1766.

(28) Goli, E.; Gai, T.; Geubelle, P. Impact of Boundary Heat Losses on Frontal Polymerization. *J. Phys. Chem. B* **2020**, *124*, 6404−6411.

(29) Firsov, A. N.; Shkadinskii, K. G. Combustion of gasless compositions in the presence of heat losses. *Combust., Explos. Shock Waves* **1987**, *23*, 288−294.

(30) Aleksandrov, V. V.; Davydenko, A. A.; Kovalenko, Y. A.; Poddubnyi, N. P. Influence of two-dimensionality of the front with heat losses on the limits of stationary gasless combustion. *Combust., Explos. Shock Waves* **1987**, *23*, 182−191.

(31) Rybanin, S. S.; Sobolev, S. L. Velocity and limits of combustion of a thermally thick condensed substance layer exchanging heat with an inert medium. *Combust., Explos. Shock Waves* **1989**, *25*, 531−540.

(32) Ivleva, T. P.; Merzhanov, A. G. Three-dimensional unsteady solid flame combustion under nonadiabatic conditions. *Combust., Explos. Shock Waves* **2003**, *39*, 300−308.

(33) Ivleva, T. P.; Merzhanov, A. G. Three-dimensional modes of unsteady solid-flame combustion. *Chaos* **2003**, *13*, 80−86.

(34) Romanov, O. Y. Critical combustion diameter. *Combust., Explos. Shock Waves* **2007**, *43*, 25−33.

(35) Lloyd, E. M.; Feinberg, E. C.; Gao, Y.; Peterson, S. R.; Soman, B.; Hemmer, J.; Dean, L. M.; Wu, Q.; Geubelle, P. H.; Sottos, N. R.; Moore, J. S. Spontaneous Patterning during Frontal Polymerization. *ACS Cent. Sci.* **2021**, *7*, 603−612.

(36) Pojman, J. A. A New Approach to Manufacturing with Frontal Polymerization to Generate Patterned Materials. *ACS Cent. Sci.* **2021**, *7*, 534−535.

⊞ Recommended by ACS